Title: Systematic review of magnetic resonance lymphangiography from a technical perspective

Abstract

Background: Clinical examination and lymphoscintigraphy are the current standard for investigating lymphatic function. MRI facilitates 3D, non-ionising imaging of the lymphatic vasculature, including functional assessments of lymphatic flow, and may improve diagnosis and treatment planning in disease states such as lymphoedema.

Purpose: Summarise the role of MRI as a non-invasive technique to assess lymphatic drainage and highlight areas in need of further study.

Study Type: Systematic review.

Population: In October 2019, a systematic literature search (PubMed) was performed to identify articles on Magnetic Resonance Lymphangiography (MRL). Field Strength/Sequence: No field strength or sequence restrictions.

Assessment: Article quality assessment was conducted using a bespoke protocol, designed with heavy reliance on the NIH quality assessment tool for case series studies and Downs and Blacks quality checklist for health care intervention studies.

Statistical Tests: The results of the original research articles are summarised.

Results: From 612 identified articles, 43 articles were included and their protocols and results summarised. Field strength was 1.5 or 3.0 T in all studies, with 25/43 (58%) employing 3.0 T imaging. Most commonly,

imaging of the peripheries, upper and lower limbs including the pelvis, (32/43, 74%) and the trunk (10/43, 23%) is performed, including two studies covering both regions. Imaging protocols were heterogenous, however T_2-weighted and contrast enhanced T_1-weighted images are routinely acquired and demonstrate the lymphatic vasculature. Oedema, vessel morphology and quantity, and contrast uptake characteristics are commonly reported indicators of lymphatic dysfunction.

Data Conclusion: Magnetic Resonance Lymphangiography is uniquely placed to yield large field of view, qualitative and quantitative, 3D imaging of the lymphatic vasculature. Despite study heterogeneity, consensus is emerging regarding MRL protocol designs. MRL has the potential to dramatically improve understanding of the lymphatics and detect disease, Further optimisation, and research into the influence of study protocols differences, is required before this is fully realised.

Keywords

Magnetic resonance lymphangiography

Lymphography

Lymphatics

Lymphoedema

Review

Introduction

Lymphoedema is a condition characterised by the accumulation of lymph in the tissue leading to chronic swelling (1). As of 2012, lymphoedema was estimated to affect as many as 250 million people worldwide, the majority of which are caused by filariasis in developing nations (2). Lymphoedema is also prevalent in developed nations; as many as 1 in 1000 Americans may be affected (1). Despite the prevalence, methods of investigating human lymphoedema are few and comparatively small numbers of medical professionals specialise in disorders of the lymphatic system (3). *In-vivo* imaging of the lymphatics may improve understanding of the underlying causes and mechanisms of lymphatic disorders, and aid diagnosis.

Lymphoscintigraphy (LS) is currently considered the clinical standard for lymphatic imaging, with direct x-ray lymphography typically phased out given its invasive nature (4). While the radiolabelled bolus used in LS is selectively taken up by the lymphatics, making it highly specific, it is limited by poor spatial and temporal resolution, and is typically limited to generating 2D projections of the main lymphatic pathways (see Figure 1) (5, 6). There is also a small radiation dose associated with LS.

Indocyanine green (ICG) lymphography, a fluorescence imaging technique (see Figure 2), overcomes the poor spatial and temporal resolution of LS and is also highly specific to the lymphatics given ICG's protein binding

properties. ICG lymphography is limited by an inability to produce 3D images and to imaging only superficial lymphatic vessels (LV)(7).

Magnetic Resonance Lymphangiography (MRL) is uniquely positioned to yield non-ionising, high spatial resolution 3-dimensional imaging of the lymphatic vasculature from head to foot, and appears capable of yielding functional characteristics of lymphatic transport (8, 9). MRL has garnered increased interest and many small cohort studies, in participants with confirmed or suspected lymphatic abnormalities, have been published (10–15). Studies investigating the technical aspects of MRL, and the complexities associated with imaging specific anatomical sites, are less common.

Optimised MRL protocols, with specific study aims, are key to unlocking MRL's potential for investigating lymphatic function. The aim of this review is to focus on the technical aspects of MRL, discussing potential pitfalls, innovative approaches, and areas in need of further research, while also highlighting any emerging consensus regarding best practice and clinical utility.

Methods

Search Strategy

A search of MRL literature was performed using PubMed with search terms: [(lymphography OR lymphangiography) OR Lymphatic angiography OR Lymph angiography] AND [MRI OR MRL OR MR-L OR Magnetic resonance*]. English language publications, published between 07/10/1999 and 07/10/2019, were included. Studies published prior to 1999 were not considered. Animal studies were not initially excluded to avoid removing articles which study both human and animal subjects. Manual literature searching provided several additional references.

Inclusion Criteria

After inspection for duplicates, vetting following the Preferred Reporting Items for Systematic Reviews and Meta-Analyses guidelines was performed (16). A single reviewer (MM) performed an initial three-stage filtering:

1. Abstracts not referencing lymphatic MRI or only lymph nodes (LN) were excluded. Single case reports, letters or replies and book chapters were also removed.
2. Full texts were retrieved and vetted with the criteria above and the requirement that scanning parameters were present.
3. Studies involving only animals were excluded, retaining those with both human and animal subjects.

Quality Appraisal

Two reviewers (MM and MvZ), with 6 and 3 years of MRI experience respectively, assessed the quality of the remaining studies using a purpose designed tool, produced with heavy reliance on the NIH quality assessment tool for case series studies and Downs and Blacks quality checklist for health care intervention studies (17, 18). Consisting of nine questions, it assessed the clarity of the imaging and contrast injection protocols, potential bias in participant selection, participant compliance and technical imaging concerns. Articles in this study are those considered of high quality, scoring ≥ 60% of the points available. Where reviewers disagreed, inclusion was by consensus, or else by a third reviewer (MB) with over 15 years of MRI experience. The full quality appraisal protocol can be found in the Supplementary Material. The article inclusion process is shown in Figure 3.

Results

Included Articles

43 articles, of an initial 612, were selected after screening and quality appraisal. Magnetic field strength was 1.5 T or 3.0 T in all studies, with 25/43 (58%) studies employing 3.0 T imaging. No human lymphatic vessel studies performed at 7.0 T were identified within any of the initial 612 articles. The most commonly imaged anatomical regions were the peripheries, upper and lower limbs including the pelvis, (32/43, 74%) and the trunk (10/43, 23%). Additionally, 3 studies were performed in the head and neck.

For all included studies, imaging and contrast injection protocols, and summary study findings, have been collated (Tables 1-4). Imaging details for non-contrast and contrast enhanced (CE) studies can be found in Tables 1-2, while Table 3 outlines contrast injection protocols. These comprehensive tables have been compiled to allow direct comparison of individual studies and show the breadth of applied methodologies.

Reported MRL protocols vary widely, however 3D heavily T_2-weighted and CE T_1-weighted sequences are commonly employed. Maximum intensity projection (MIP) reformatting of the entire imaged volume, including MIP images from each phase of dynamic CE-MRL studies, is employed to aid visualisation of the enhancing structures.

Non-Contrast T_2-weighted Imaging

A fluid-sensitive heavily T_2-weighted fast/turbo spin echo (FSE/TSE) sequence (note that the generic term 'rapid acquisition with relaxation enhancement, or RARE, is also in use), similar to those used to image the biliary system, is performed in the vast majority of studies acquiring non-CE images (22/29, see Table 1). *Ex-vivo*, the T_2 time of lymph has been measured at 610 ms (3.0 T) and hence can be expected to retain reasonable signal in heavily T_2-weighted images (9). An example T_2-weighted MRL image of the lower limbs clearly displaying LVs can be seen in Figure 4. Typical timing parameters for these sequences are of the order Repetition / Echo time (TR/TE) = 3000-4000 / 500-700 ms at both 1.5 T and 3.0 T with voxel sizes typically >1 mm^3 (Table 1). Image acceleration techniques such as partial Fourier acquisitions and use of parallel imaging were reported in eight studies employing T_2-weighted spin echo sequences (eleven studies in total, as shown in Table 1), however the effect on acquisition time is unclear as this was rarely reported. In those which do, 2-11 minutes acquisitions have been reported (see Table 1).

Individual studies employed arterial spin labelling (ASL), time of flight (TOF) and steady state free precession (SSFP) techniques to achieve specific goals such as detecting lymphatic flow in the meningeal lymphatics, estimating the speed of lymphatic flow and to acquire venographic images.

Contrast Enhanced T1-weighted Imaging

Paramagnetic gadolinium-based contrast agents (GBCA) have been shown capable of reducing the long native T_1 time of lymph sufficiently to produce high signal intensity T_1-weighted images, as demonstrated for the thoracic duct in Figure 5. Dynamic imaging, demonstrating temporal changes in contrast distribution, is common, with volumes acquired in 30-180 seconds (Table 2).

Short TR and TE 3D spoiled gradient echo (SPGR) sequences, with typical scanning parameters of TR/TE/ = 3-6 ms / 1-2 ms and Flip Angle (FA) =12-30^o regardless of field strength, were most often employed (24/33). Image acceleration techniques were rarely reported in these studies; only one study employing SPGR indicated the use of partial Fourier, while four studies employed parallel imaging. Signal-to-noise ratio (SNR) in CE T_1-weighted images appears superior to T_2-weighted ones: Crescenzi *et al.* reported SNR of approximately 10 in the arm and torso LVs using T_2-weighted TSE at 3.0 T (19), while Mazzei *et al.* measured peak SNR in leg LVs of >250 with a CE SPGR sequence at 1.5 T (20). Spatial resolution is also typically superior in T_1-weighted images compared to T_2-weighted with voxel sizes ~ 1mm^3 reported regularly.

Dixon based imaging is performed by some authors as a proactive fat suppression technique and by others employing the use of a contrast agent to supress signal from blood vessels.

Contrast Injection Protocol

Six different GBCAs were employed within the included studies (Table 3). These agents were often combined with local anaesthetic for pain relief, and in one case a small volume of a vasoconstrictor to test if this reduced undesirable venous enhancement (21); a common issue for peripheral CE-MRL. Gadopentetate dimeglumine and gadobenate dimeglumine were the most often employed GBCAs (eleven and ten instances respectively), while the use of gadoterate meglumine was only described in a single study.

When performing CE studies in the peripheries, between 2-5 injections of ~1mL GBCA solution is delivered into the digital web spaces, either intradermally or subcutaneously, with small gauge (e.g. 24G) needles. In the trunk (i.e. from pelvis to neck) larger volume injections (e.g. 2-8 ml) administered via the inguinal lymph nodes were more common.

Massage of the contrast injection site was performed in approximately half of peripheral MRL (pMRL) studies, often citing research demonstrating improved contrast uptake into the lymphatics of rabbits (22). Massage durations varied between 0.5-5 minutes.

Clinical Value

Visualisation of lymphatic vessels is common in T_1-weighted studies, even in healthy limbs (23–25), as is recording their abundance and size.

T_2-weighted studies appear particularly sensitive to the detection of areas of fluid accumulation, and the presence of the so called honeycombing pattern (Figure 6), thought to be a marker of tissue fibrosis (26). Lymphatic vessels

are also visualised in T_2-weighted images, however this may be improved by specific image optimisation: Crescenzi *et al.* acquired images at 3.0 T with a range of echo times and were only able to clearly visualise LVs at TE = 121 ms, an echo time much shorter than is typical (27).
Lymphatic vessels are often reported as being larger in participants with lymphoedema, and regions of dermal backflow (rerouting of lymphatic fluid to the dermal lymphatics) are regularly observed (Figure 7).

Dynamic CE studies regularly document the temporal nature of lymphatic enhancement (e.g. time to peak signal, or signal vs time curves), with two authors reporting lymph flow speed estimates: Liu *et al.* estimated speeds between 0.3 – 1.48 cm/min in the legs of primary lymphoedema participants, while Borri *et al.* recorded a speed of 9.7 cm/min in the arm of a single participant with breast cancer related lymphoedema (BCRL) (8, 28). Rane *et al.* measured lymph speed in the arms of healthy controls and BCRL patients using pulsed arterial spin labelling. Altered lymph dynamics were demonstrated, with a reduction in lymph speed observed in the affected vs. unaffected arms of patients; mean = 0.61 ± 0.22 cm/min vs 0.48 ± 0.15 cm/min (9).

Kuo *et al.* were able to demonstrate lymph flow in the head, adjacent to the superior sagittal sinus (SSS), via time of flight imaging (29). Employing spatially selective saturation bands, the direction of flow within the

meningeal lymphatics was also demonstrated as being counter to the blood flow of the SSS.

Table 4 summarises common findings in the included studies.

Comparisons to Lymphoscintigraphy

Several studies include comparisons of the performance of MRL with Lymphoscintigraphy and comment on the concordance between imaging findings across modalities. In all studies, improved LV visualisation with MRL in the limbs was reported (5, 6, 23, 30). Improved detection of inguinal lymph nodes was reported by Liu *et al.* when comparing CE-MRL to LS (16/17 vs 9/17 patient images displaying inguinal nodes for CE-MRL vs LS), while Notohamiprodjo *et al.* report the converse (6, 30). In a study considering LS as the gold standard technique, Weiss *et al.* reported sensitivity and specificity values of 68% and 91% for detection of focal lymphatic lesions (e.g. lymphocele or dermal backflow) by CE-MRL compared to LS (5). Figure 1 shows example LS and MRL images from the same participant.

Site Specific Considerations

Peripheral MRL (pMRL)

MRL has been successfully performed in the arms and legs of participants diagnosed with lymphoedema (Figures 1,4,6-7) and healthy participants (Figure 8).

Contrast enhanced pMRL is susceptible to the contaminant enhancement of venous structures alongside the lymphatics however. Despite some authors reporting no difficulty distinguishing enhancing veins from lymphatics based on their appearance, others indicate that venous signal complicates anatomical labelling of enhancing structures (20, 31, 32). Consequently, multiple attempts have been made to proactively reduce the influence of venous enhancement, including: waiting for the venous enhancement to subside (28, 33); collecting a venogram to identify veins (31, 34); injection of ultrasmall superparamagnetic iron oxide (USPIO) for venous suppression (35, 36); or reducing the injected GBCA concentration (8) (additionally reducing T_2 related signal loss at the injection site, observed as early as 2006 (37)).

Given the short T_1 time of fat, the majority of T_1 weighted contrast enhanced pMRL studies are performed fat suppressed (Table 2).

MRL of the Trunk

MRL imaging of peripheral lymphatics has been an active area of research at least since the early 1990's (see for example Case *et al.,* 1992 (38)), however imaging the lymphatics of the trunk appears not to have been explored until toward the end of that decade (39). Much of the research has focused on imaging the pathway from the two lumbar lymphatic trunks through to the termination of the thoracic duct (TD). Figure 3 shows an example of normal appearing TD anatomy, while Figure 9 demonstrated a narrowed TD and leakage in a patient diagnosed with chylothorax.

The effect of cardiac and respiratory motion is addressed by many studies imaging the lymphatic vessels in the trunk. Reducing respiratory motion by acquiring data while participants hold their breath is performed in several T_1 weighted sequences, however for lengthy T_2-weighted sequences respiratory gated and cardiac triggered sequences are often preferred (Tables 1-2).

CE studies in the trunk are often acquired after contrast injection into the inguinal lymph nodes, with needle positioning requiring ultrasound or x-ray guidance (40, 41). Fat suppression techniques were applied in 2/4 contrast enhanced studies of the trunk, but only one T_2-weighted.

MRL of the Head

Only three studies imaging the head were included in this review, however they demonstrate the ability to detect lymphatic structures in the face, neck and cranial meninges (21, 29, 42). Two studies perform CE-T_1 imaging while non-contrast time of flight (TOF) imaging was performed by Kuo *et al.* (29). Figure 10 shows an example TOF image. Similar to pMRL, Loo *et al.* reported both enhancement of venous structures, and signal loss at the injection site where GBCA concentration is largest (21).

MRI studies have begun to investigate the existence and function of a recently hypothesised fluid system in the brain: the glymphatic system (43, 44). As the name suggests, the glymphatic system (derived from the terms glial and lymphatic) is considered to clear waste from within the brain, as the lymphatic system does throughout the rest of the body, via the cerebrospinal fluid (CSF). Within the glymphatic model, CSF flow is not

within an independent vascular system but instead occurs in the perivascular space (unique to neural vasculature) surrounding neural vessels, and is driven by pressure induced from arterial pulsation (43, 44). The CSF then passes through the brain parenchyma, picking up proteins during this passage, before reaching the perivascular space around the veins and so clearing waste products from the brain. Dysfunction of this drainage pathway has been hypothesised to be linked to neurodegenerative diseases such as Alzheimer's and Parkinson's (45). The discovery that drainage of waste from the brain occurs not only via perivascular space surrounding veins, but also through a meningeal lymphatic system to the cervical lymph nodes, demonstrates the connection between these systems (46). Given the connection to the glymphatic system and hence potential involvement in neurodegenerative disease processes, and the demonstration of MRI to investigate this system in humans, the number of studies reporting meningeal lymphatic MRI is only likely to increase (29, 47).

Discussion

This review provides evidence that MRI of lymphatic vessels is viable across the entire body and is capable of demonstrating not only morphological changes with disease, but also altered flow dynamics. There remain no standardised protocols for MRL, however T_1-weighted SPGR post intradermal / subcutaneous injection of standard GBCA, and non-contrast T_2-weighted sequences may be considered standard approaches.

In an attempt to assist readers considering MRL, the remainder of this section is dedicated to the discussion of key technical considerations of MRL protocols and potential avenues of research.

Spatial and Temporal Resolution

The small size of lymphatic vessels demands high spatial resolutions for visualisation, which limits temporal resolution without advancements in MR hardware (field strength, coil sensitivity etc.) and k-space sampling techniques. Clinicians and researchers should therefore consider which of these parameters is most important when planning MRL studies.

Spatial Resolution and Lymphatic Vessel Visualisation

Lymph vessels are typically sub-mm in diameter, with only the larger trunks and ducts reaching the mm scale (48). Compared to 2D, 3D MR acquisitions facilitate thinner slices with less severe partial volume artefacts (also improving SNR for the same effective slice thickness), but increases acquisition times. Gibbs ringing artefacts, series of lines in the image at abrupt signal boundaries such as bright contrast-enhanced lymphatic vessels and low signal background tissue, may be seen propagating in the slice encoded direction in 3D acquisitions. This is often not observed unless multi-planer reformatting is performed however (49). Regardless of these ringing artefacts, 3D acquisitions are preferable in studies aiming to visualise individual lymphatic vessels, especially in healthy volunteers, or when estimating LV size.

T_2-weighted images with relatively low resolutions (~ 2-3 mm isotropic) appear adequate to identify lymphoedematous regions, so improvements of spatial resolution may not be necessary for these already lengthy sequences. If higher resolutions are desired, performing FSE/TSE sequences including a driven equilibrium (DE) pulse may be preferred. In DE sequences, a 90° radiofrequency (RF) pulse at the end of the sequence returns transverse magnetisation to the longitudinal plane, recovering transverse magnetisation faster than normal T1 relaxation alone. This may therefore accelerate imaging when coupled with reductions in TR, and so be used to offset the increased acquisition time required when increasing image resolution (50). Arrivé *et al.* (51) and Jeon *et al.* (52) employed DE when imaging the limbs of participants diagnosed with lymphoedema.

Lymphatic Contractions and Lymph Transport

Lymphatic contractile frequencies have been estimated at 1.39 – 6.78 contractions/min in the TD and ~5 contractions /min at rest in superficial leg lymphatic collector vessels (53, 54). These pulsation frequencies are beyond even the most rapid imaging uncovered in the review. Whether it is possible using MRL to measure transient signal changes related to lymph transport, a proxy for lymph pulsation frequency, is yet to be explored, but would require high spatial and temporal resolutions.

The signal-to-noise ratio (SNR) required would also likely need to be improved, especially when imaging at higher resolution (which lowers SNR), in order to detect the signal changes associated with lymphatic propulsion.

Imaging at field strengths > 3.0 T, and the application of advanced acquisition techniques such as compressed sensing (55), would prove beneficial to enable the required spatial resolution, SNR and accelerated data acquisition.

Physiologically relevant flow measurements have been acquired from MRI datasets however. Measurements of bulk bolus speed (see Table 4), estimated in three studies using either CE or ASL techniques (8, 9, 28), demonstrate the potential of MRI to monitor lymph flow and may prove beneficial for characterising lymphatic physiology and diagnosing lymphatic disorders.

Motion Artifacts

Heavily T_2-weighted TSE/FSE images remain susceptible to motion artefacts given the long TE required. Imaging lymphatics within the torso has focused on the TD; an area susceptible to the effects of both cardiac and respiratory motion. Proactive steps can be taken to mitigate this issue, including breath-held acquisitions. Krishnamurthy *et al.* found it necessary to intubate and sedate their participants as age or existing morbidities prevented adequate breath holds (40). Respiratory gating and cardiac triggering have been successfully employed in some of the studies reviewed here, but can elevate total imaging time (40, 41, 56–60). Accelerating imaging, via k-space reduction techniques or use of DE for example, may also reduce the likelihood and magnitude of bulk motion artefacts, however

signal loss due to spin dephasing across the lengthy echo train of TSE/FSE will persist.

Lymph Signal and Background Signal Suppression

MRL image contrast and signal must be sufficient to both identify lymphatic vessels and distinguish them from other body tissues. Although the SNR in T_2-weighted images appears much lower compared to CE-T_1 studies, lymph vessels have been visualised in both.

Image optimisation is a non-trivial process and in general MR sequence timing parameters vary as a function of field strength (B_0): both T_1 and T_2 values of tissues are B_0 dependant, typically increasing and decreasing respectively with increases in B_0. It is interesting to note the similarity in sequence parameters for both CE-T_1 and non-contrast T_2 studies regardless of field strength. This may have arisen as a result of empirically determined optimal sequence parameters, however this is not commented on within the literature. There is markedly little discussion of optimisation of TR / TE within the articles included in this study: adequate image quality with the same protocol despite changes in field strength, and a lack of reported lymph vessel T_1 and T_2 times required for robust prospective protocol optimisation, may explain the lack of studies documenting image optimisation (27, 61).

Flip angle optimisation for dynamic CE studies is also non-trivial and requires clear goals; flip angle choice may be different if image contrast or dynamic range are to be optimised for example. Higher flip angles maximise

T_1 weighting, but with an increased potential for generating higher residual fat signals (62). Flip angles in the range 10-30^o have been reported in CE studies, with none detailing in-depth flip angle optimisation.

When imaging in fatty regions, fat suppression techniques can also improve contrast-to-noise ratio (CNR) and lymph conspicuity, and techniques insensitive to inhomogeneities in the RF field (also referred to as B1 field inhomogeneities) such as Dixon or Spectral Attenuated Inversion Recovery (SPAIR) are often employed. Dixon methods resilient to B_0 inhomogeneities have been developed and so may be considered preferable for fat suppression. Acquiring the multiple images required for Dixon studies can increase scan times substantially, however multi-echo Dixon acquisitions reduce this time penalty (49, 63). Pieper *et al.* performed 3D multi-echo Dixon imaging in participants at 1.5 T. With a resolution of 1.0 x 1.2 x 2.5 mm, they imaged the entire torso with three image stacks requiring 10s each (64). Further studies investigating the use of Dixon based methods across the entire anatomy are required, however when robust fat suppression is needed Dixon imaging should be considered.

Although no 7.0 T studies of the lymphatic vessels were uncovered in this review, the feasibility of *in-vivo* human lymph node imaging at 7.0 T has been demonstrated (65–67). Freitag *et al.,* performing T_2-weighted TSE at 7.0 T, highlighted the presence of lymph vessels connected to LN in their high resolution (0.2 x 0.2 x 2 mm) images, emphasising the utility of ultra-high field strength imaging to generate high resolution images with sufficient

signal to depict both lymphatic nodes and vessels (67). Imaging at 7.0 T may also enhance visualisation of LVs in healthy limbs which remains difficult at 3.0 T (24, 68).

Differentiating Lymphatic and Venous Structures

Differentiating venous and lymphatic structures appears a systemic issue amongst CE studies. Using vessel morphology or signal enhancement as potential discriminators between LV and veins is commonly reported, however many authors raise concerns that this approach is insufficient and may decrease the specificity of MRL (20, 31, 32).

Acquiring separate venographic images, with or without contrast, may improve visual conspicuity of veins or be used as subtraction masks for MRL data. Image registration may be necessary to reduce potentially confounding subtraction artefacts however (8, 34). Non-contrast venograms were produced using balanced steady state free precession (bSSFP) by Mazzei *et al.*(20). The large T_2/T_1 ratio of lymph raises the possibility of the presence of lymphatic vessels in these venograms however, as bSSFP image contrast is T_2/T_1 weighted (69).

The administration of separate USPIO agents in the bloodstream can suppress venous signal by drastically reducing T_2 times, allowing a selective lymphographic image to be generated (35, 36). At the time of writing, the agent used in these studies is not licenced for use as an MR contrast agent by the U.S. Food and Drug Administration (FDA) or the European Medicines Agency (EMA). It should be noted that administration of GBCA via skin

injection is also considered ‘off-label’, however the safety of GBCA delivered by intravenous injection is well established. The risks of GBCA administration (allergy, Gadolinium retention in body tissues, and development of a rare but serious condition in those with renal function: nephrogenic systemic fibrosis or NSF) should always be carefully considered prior to injection regardless of route of administration (intravenous or intradermal). Macrocyclic agents such as gadobutrol, gadoteridol and gadoterate meglumine, should be preferred given their superior safety profiles (70).

Protocols employing contrast agents to act specifically on venous blood introduce additional safety concerns associated with multiple contrast injections. Large reductions in contrast agent dose, as employed by Borri *et al.*, have the effect of both reducing the potential hazards associated with GBCA delivery and the intensity of venous signal. This, however, has only been demonstrated in a small pilot cohort of subjects (8). Alternatively, waiting until the venous signal has decreased, but lymphatic enhancement remains, has been suggested to be a simple and effective solution (28). Observation of temporal behaviour of lymphatic transport within this wait period may be lost, however estimations of bulk bolus speed should still be possible.

Contrast Agent Delivery

Six GBCA agents, half of which (gadopentetate dimeglumine, gadodiamide and gadobenate dimeglumine) have had their use restricted within the EU

(70), were used within the CE studies. Only one publication investigated the use of different GBCAs (gadoteridol and gadopentetate dimeglumine), concluding that enhancement was equivalent (21). This study was conducted in the head and so caution is advised when drawing on these finding when imaging the limbs and trunk. Other articles comment on parameters of GBCAs which may make them optimal for LV studies, such as higher molecular concentration or higher protein binding (10, 31, 71). A large body of research exists regarding contrast agent use in LN imaging (see for example "MR Contrast Agents in Lymph Node Imaging" (71)), much of which will be relevant to LV imaging, however specific studies investigating the use of different contrast agents for LV imaging are still required.

Injected Solution and Contrast Mobilisation

GBCA is most commonly administered undiluted in CE studies, however as described previously Borri *et al.* propose injections heavily diluted with saline such that each mL of injected solution contained 0.02mL of contract agent, 0.1mL of anaesthetic and 0.88mL saline (8). Krishnamurthy *et al.* also diluted their GBCA with saline when performing intra-nodal injections, using a 1:1 dilution in older patients and a 1:2 GBCA to saline dilution in younger patients. This was performed in order to reduce T_2 dephasing effects of the GBCA (40). Loo *et al.* investigated the effect of delivering contrast undiluted vs diluted and different injection volumes, finding that dilution of GBCA with an equal volume of sterile water, and smaller

injections of 0.3-0.5mL per injection, provided optimal lymphatic enhancement in the head (21).

Massage proximal to the contrast injection site is common after intradermal/subcutaneous contrast injection, but there is no clear consensus as to how, or if, to add an intervention to improve contrast mobilisation into the lymphatics. Loo *et al.* demonstrated that repeated massage extended the time over which LV enhancement was sustained and produced additional signal peaks (21), perhaps due to increased interstitial pressure from the massage driving contrast into the lymphatics (72, 73). Pieper *et al.* requested that participants move their limbs after contrast injection, presumably in an attempt to increase contrast uptake, a method employed regularly for ICG and lymphoscintigraphy (64). The extent to which this changed contrast uptake was not explored however.

While clear that standard GBCAs can be used for LV imaging, variable number of injection sites, injected volume and GBCA formulation have been employed, and more research is required before an optimal injection protocol can be recommended. A systematic exploration of the effect of different injection and intervention (e.g. massage) protocols, on contrast uptake, study repeatability, and to what extent subtle lymphatic insufficiencies could be masked, are needed (74–76).

Quantitative Analysis

MRL has been shown to visualise structural abnormalities of the lymphatic system, with additional quantitative analyses differentiating healthy and

abnormal groups. Common measurements include counting visible LVs, estimating vessel diameter, and recording signal enhancement characteristics.

Many studies use the contralateral limb as an internal control in both qualitative and quantitative studies. The results of such comparisons should be approached with caution as abnormal imaging signs within the contralateral limb have been observed (58, 77). Enrolment of a healthy matched control cohort would reduce the risk of such confounders.

Vessel Size

The thickness of the TD has been estimated by multiple authors, often enrolling participants with non-lymphatic specific abnormalities such as liver malignancy and a Fontan circulation (56, 58), with diameters in the region of 1-7 mm observed. Larger peripheral LVs in individuals with lymphatic disease have also been commonly observed compared to healthy controls.

Regardless of anatomy, absolute measurements of LV diameter will be prone to error when voxel sizes are similar to, or greater than, the vessel size. Acquiring higher spatial resolution images will improve the accuracy with which LV sizes can be estimated. For large field of view studies, ~ 1 mm^3 voxels may be approaching the maximum feasible resolution for current clinical MR systems. Imaging at higher field strengths and employing acceleration techniques such as compressed sensing and multiband RF

imaging to improve image resolution should be considered if more representative estimates of vessel size are required.

Lymph Flow and Contrast Distribution

Time to peak lymphatic enhancement has been estimated in multiple CE studies. These values will likely depend on measurement location and injection protocol (e.g. contrast agent, dose, massage etc.), and are hence difficult to compare directly.

Lymphoscintigraphy has long been used to estimate lymph drainage by determining tracer uptake in the lymph nodes (78). Although not explored in any of the articles reviewed here, similar measurements may be possible via MRL with T_1 measurements in the lymphatic vessels or lymph nodes yielding estimates of local GBCA concentration. This requires that sufficiently low injected GBCA concentrations and high flip angles are employed to ensure a linear relationship between image signal and $1 / T_1$ is maintained. Estimates of T_1 will be affected by factors such as fluid flow and diffusion, partial volume, changes in local proton-density and field inhomogeneities, and so will require good experimental design (79, 80). Lymph speed has been estimated in the limbs by three studies employing different MRL methods and analysis models. With an ASL based approach, measuring signal as a function of post-labelling delay time, lymph speed in the arm was estimated from signal in a downstream LN in the arms of BCRL patients (9). Imaging the leg, Liu *et al.* recorded lymph speeds consistent with those achieved with ASL by measuring lymphatic vessel length on CE

images and calculating speed as enhanced vessel length divided by the acquisition time (28). Borri *et al.* recorded slightly higher speeds in their single participant with BCRL (8). A five-parameter modified logistic model was employed to fit signal enhancement, with one parameter representing the GBCA arrival time. It is interesting to note that despite the methodological differences, reported speeds are similar (~ 0.5 - 2 cm/min) for affected limbs across these studies.

Is MRL superior to ICG and lymphoscintigraphy?

Lymphoscintigraphy is currently considered the clinical gold standard for diagnostic lymphatic imaging. Given the sparsity of studies comparing techniques directly, or high-level evidence such as meta-analyses, it is difficult to conclude which technique is superior. However, it is interesting to note that all studies within this review comparing MRL and LS report improved LV visualisation in the limbs with MRL (5, 6, 23, 30). The superiority of MRL may also become more evident with further optimisation.

It is perhaps more pertinent to comment on the complementary nature between MRL, LS and ICG lymphography, and a combination of MRL with either may deliver a more complete understanding of lymphatic anatomy and physiology than MRL alone. While ICG yields high spatial and temporal imaging of superficial lymph vessels, which may lead to estimations of vessel contraction frequency, MRL facilitates evaluation of the lymphatic system over large anatomical regions and can image both superficial and deep lymphatic structures such as the thoracic duct (58, 81).

Lymphoscintigraphy, while lacking spatial and temporal resolution, is readily quantifiable to estimate tracer clearance and hence lymphatic transport. Studies of lymphatic transport by MRI are being performed, both non-contrast (using an ASL approach) and contrast enhanced. Further studies are required before MRL studies of lymphatic transport can be interpreted with a high degree of confidence, and routinely implemented however.

Conclusion

In conjunction with basic biological research and imaging techniques such as ICG lymphography, lymphoscintigraphy and histology, MRL can become a powerful tool in gaining a more detailed understanding of the complexities of the lymphatic system. The potential for MRL research to directly influence clinical practice in diseases of the lymphatic system was recently demonstrated in an article reporting 92% sensitivity in identifying lymphoedema with MRL alone (77). Studies investigating factors such as: the influence of administered contrast agent formulation and massage on contrast uptake characteristics; optimal imaging parameters for T_2-weighted depiction of lymphatic vessels; and relevance of quantitative image makers such as estimates of lymph speed and vessel size to lymphatic function, are still required to truly unlock MRLs diagnostic and prognostic potential.

Figures

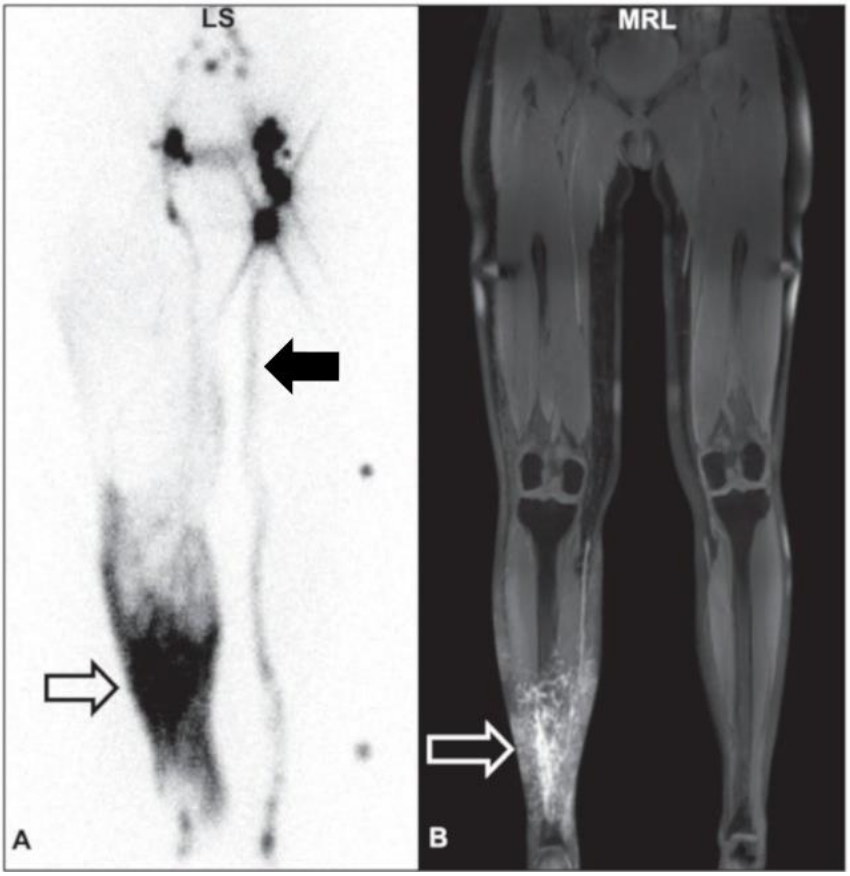

Figure 1. Lymphoscintigram (A) and Magnetic Resonance Lymphangiogram (B) acquired in the lower limbs of a participant with lymphoedema of the right lower limb. MRI was acquired after contrast injection in the affected limb with a contrast enhanced 3D T_1 weighted gradient echo sequence with TR/TE = 4.13 / 1.47 ms, flip angle = 25°, reconstructed voxel size = 0.80 x 0.80 x 0.80 mm. Both modalities show regions of dermal reflex (open arrows). The lymphoscintigram also shows a normal appearing main lymphatic pathway leading to the inguinal lymph nodes in the unaffected (left) limb (filled arrow). Reproduced with permission (5).

Figure 2. Lower limb Indocyanine Green (ICG) fluorescence image, showing the lateral aspect of the shin, in a participant with unilateral lower limb lymphoedema acquired at St George's, University of London. ICG binds to proteins such as albumin making imaging specific to the lymphatics. This image was produced via laser excitation of the ICG after intradermal injection between the digital webspaces, and subsequent detection of the fluorescence by a CCD detector. ICG imaging's high spatial resolution allows identification of individual superficial lymphatic vessel (solid arrow), however emissions from deeper lying structures are quickly attenuated. In the unaffected individual, fairly linear vessel pathways flowing distally to proximally, and following known anatomical pathways, should be observed. In an affected

state an abnormal drainage pattern is evident such as no flow, medial to lateral (or vice versa) flow, and dermal rerouting (dashed arrow). Image "Lower limb ICG in unilateral lymphoedema" shared by St George's, University of London, under the CC BY-SA-4.0 International licence (https://creativecommons.org/licenses/by-sa/4.0/), https://commons.wikimedia.org/wiki/File:Lower_Limb_ICG_in_unilateral_lymphoedema.tif.

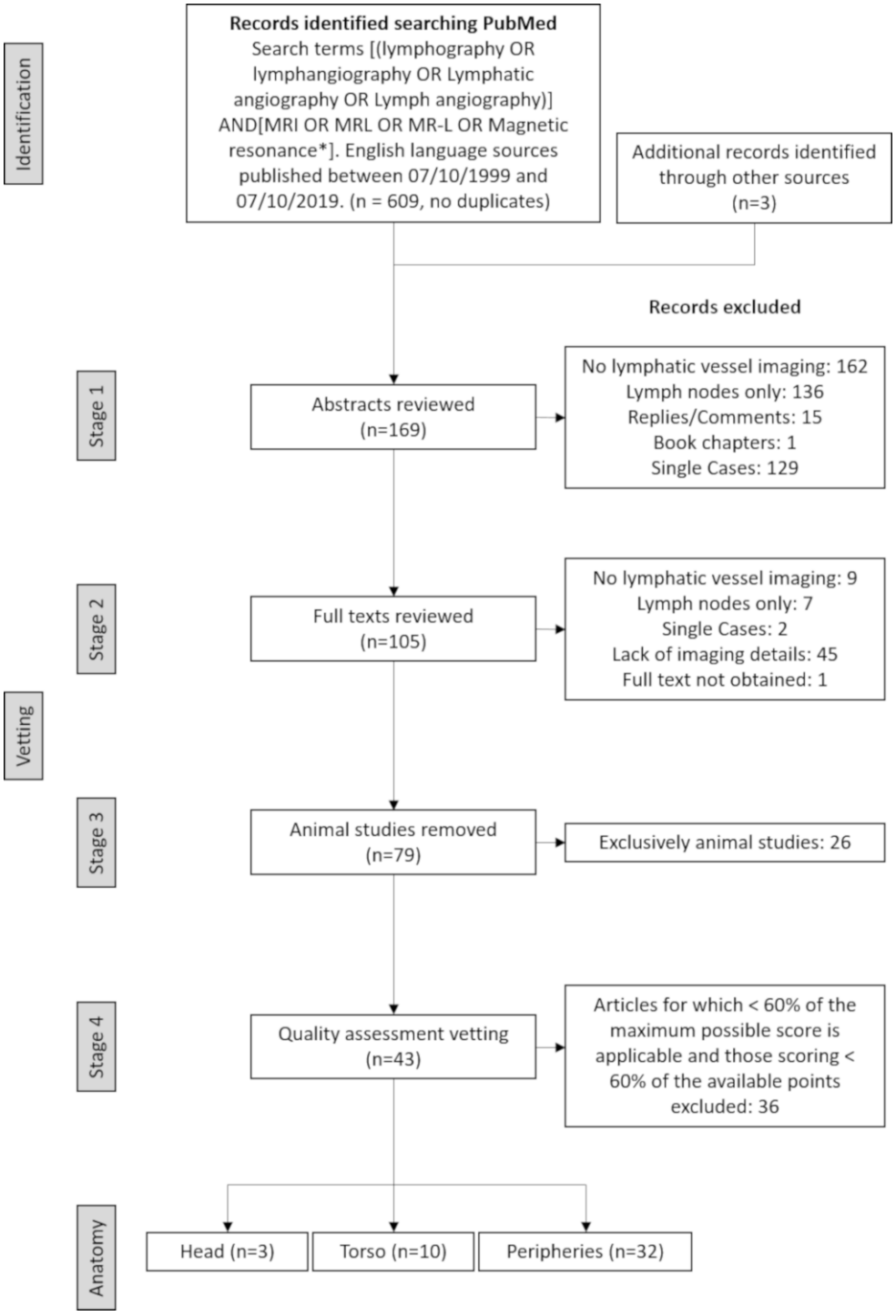

Figure 3. Study selection flow chart. PubMed revealed 609 English language sources after a search for lymphatic vessel Magnetic Resonance Imaging. After vetting and quality assessment, a total of 43 articles were included in this review, the majority of which report imaging in the limbs and/or pelvis (collectively labelled the 'peripheries'). Note that some studies cover both the

torso and the limbs and so are counted twice. One study, performing peripheral MRL and a single case of torso MRL, was included for review with the single torso case excluded.

Figure 4. Maximum intensity projected T_2-weighted non-contrast MRL image of a participant with unilateral lymphoedema of the left leg. TR/TE = 4000/884 ms, flip angle = 90°, voxel size = 0.8 x 1.4 mm, acquired with a driven equilibrium pulse. Many tortuous vessel-like structures are seen in the left leg (solid arrows), with signal intense areas of fluid accumulation seen by the left ankle (dashed arrows). High signal structures are also observed at the right ankle (diamond headed arrow). The high signal in the vessel-like structures seen in the left limb may be due to vessel dilation and/or fluid stasis, both of which can occur as a result of pathology. Reproduced with permission (51).

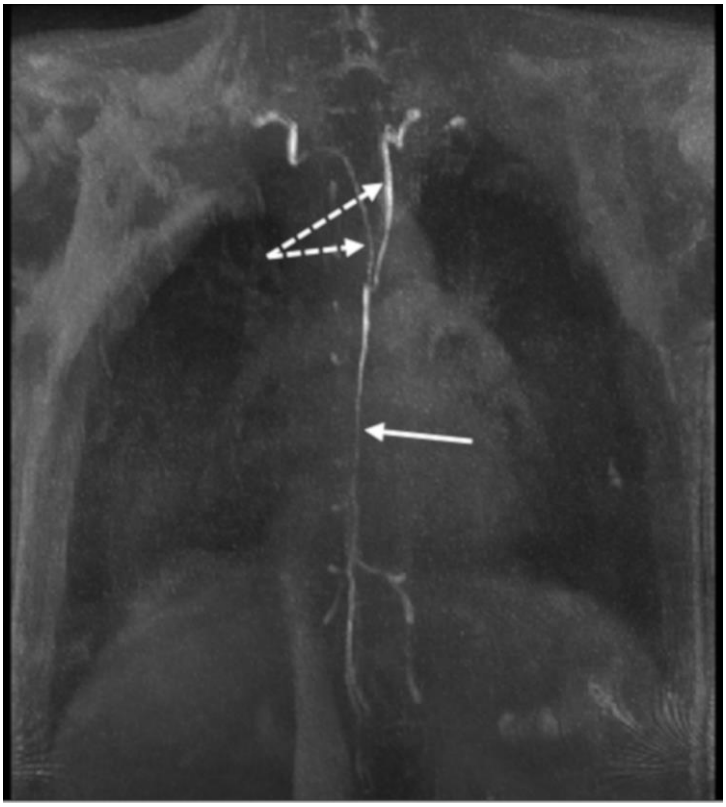

Figure 5. Thoracic duct MRL of a participant with bilateral upper and lower limb lymphoedema acquired with a contrast enhanced T_1-weighted SPGR at St George's, University of London. TR/TE = 5.2 / 1.8 ms, flip angle = 30°, reconstructed voxel size = 0.75 x 0.75 x 1.50 mm. This maximum intensity projection clearly displays contrast draining through a single smooth channelled thoracic duct (solid arrow), which appears to bifurcate and drain bilaterally (dashed arrows) toward the subclavian vein. Image "Thoracic duct MRL in lymphoedema" shared by St George's, University of London, under the CC BY-SA-4.0 International licence (https://creativecommons.org/licenses/by-sa/4.0/), https://commons.wikimedia.org/wiki/File:Thoracic_duct_MRL_in_lymphoedema.tif.

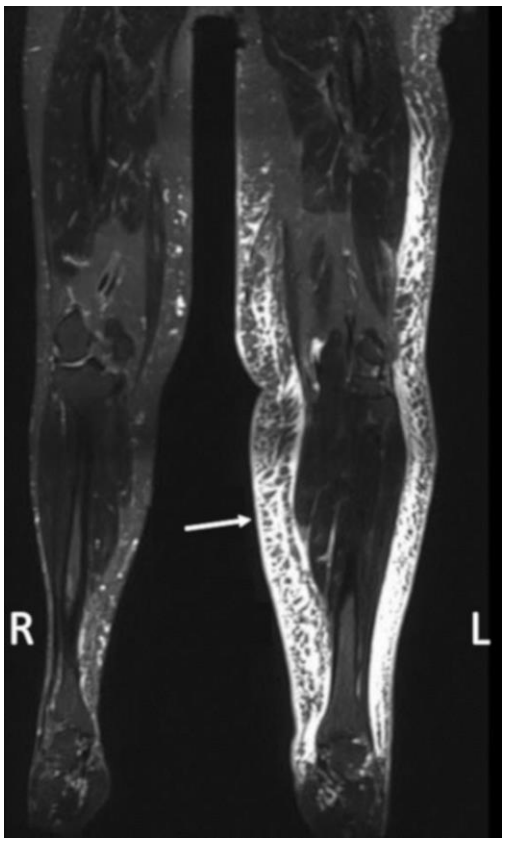

Figure 6. T_2-weighted TSE image of a participant with lower limb lymphoedema in the left limb demonstrating a clear honeycomb pattern of the subcutaneous tissue (arrow). Acquired with TR/TE = 2870/797 ms, voxel size = 1.1 x 1.0 x 1.0 mm. Reproduced with permission (82).

Figure 7. Contrast enhanced image of the left arm of an individual with lymphoedema showing a region of dermal backflow, the rerouting of lymph to the dermal lymphatics. Acquired with a fat suppressed SPGR, TR/TE = 3.5/1.3 ms, flip angle = 14.9^{o}, voxel size = 1.0 x 1.4 x 1.2 mm. Reproduced with permission (23).

Figure 8. Lower limb MRL of a healthy participant imaged with a fat suppressed contrast enhanced T_1 weighted SPGR at St George's, University of London. TR/TE = 3.6 / 1.6 ms, flip angle = 12°, reconstructed voxel size = 0.75 x 0.75 x 0.75 mm. This maximum intensity projection demonstrates thin, discontinuous appearing, lymphatic vessels (solid arrow), as well as larger venous structures (dashed arrow). Image "Lower limb MRL in healthy participant" shared by St George's, University of London, under the CC BY-SA-4.0 International licence (https://creativecommons.org/licenses/by-sa/4.0/), https://commons.wikimedia.org/wiki/File:Lower_Limb_MRL_in_healthy_participant.tif.

Figure 9. Lymphatic leakage (solid arrow) and thoracic duct narrowing (dashed arrow) identified 12 mins into imaging of a patient with recurrent chylothorax. Acquired with a fat suppressed SPGR, TR/TE = 4.0/1.9 ms, flip angle = 10°, voxel size = 1.0 x 1.4 x 1.2 mm. Reproduced with permission (40).

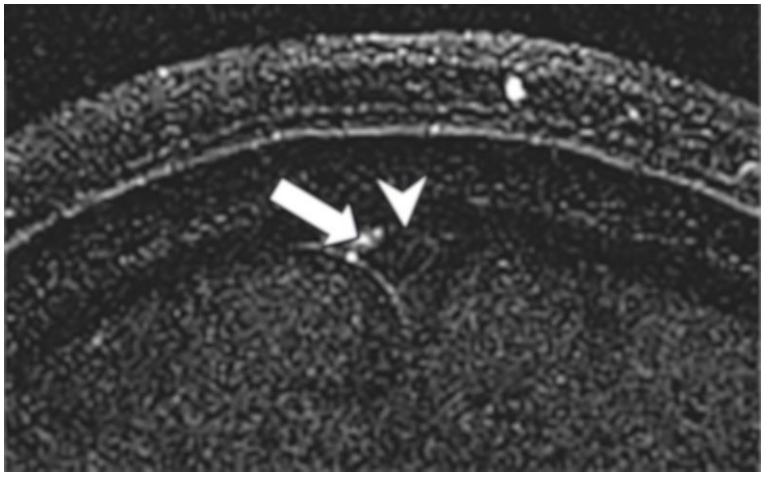

Figure 10. Time of flight (TOF) image in the head of a healthy volunteer showing signal in the meningeal lymphatics (arrow) and low signal in the superior sagittal sinus, SSS, (arrow head). Image produced with TR/TE = 30/4.49 ms, flip angle = 10^{o}, voxel size = 0.31 x 0.31 x 1.5 mm, and subtracting images acquired with saturation bands anterior and posterior to the SSS from those acquired with a saturation band only anterior to the SSS. Reproduced with permission (29).

Tables

Table 1. Non-contrast lymphatic sequences, excluding those acquired for node visualisation. All studies are T_2-weighted unless otherwise stated. Where field of view and matrix are present, but voxel sizes not stated, calculated voxel sizes are displayed. The Fat Suppressed column indicates if a fat suppression pre-pulse was used; Dixon imaging or water frequency selective excitations is not considered as such.
** - values quoted from imaging affected participants. Variations in protocol between affected and unaffected participants can be seen in the original article.*

Anatomical region	**Field strength (T)**	**Sequence variant**	**TR/TE (ms)**	**Flip angle (°)**	**Acquisition time (min:sec)**	**Resolution**		**Additional parameters**			**Source**
						In-plane Matrix	**Reconstructed Voxel (mm)**	**Fat Suppressed?**	**Motion Reduction**	**Other**	
Head and Neck	3.0	Flow weighted TOF	30 / 4.49	10	-	160 x 160	0.31 x 0.31 x 1.5			Anterior and posterior saturation bands, NSA =10	(29)
Torso	1.5	3D FSE	3000-6000 / 500	-	-	320 x 320	1.1 x 1.1 x 2.0		Respiratory gated	Partial Fourier	(56)
Torso	1.5	3D TSE	2500 / 650	140	2-5	256 x 256	1.1 x 1.1 x 1.1		Respiratory navigated, cardiac gated		(57)
Torso	1.5	3D TSE	2500 / 650	140	2-5	256 x 256	1.2 x 1.2 x 1.2		Respiratory navigated, cardiac gated		(41, 59)
Torso	3.0	-	2000-4500 / 550-750	-	5-10	320 x 256	1.2-1.4 x 1.5-1.8 x 1.0-2.0				(83)
Torso	3.0	3D TSE	3000 / 600	110	10:51	-	1.39 x 1.39 x 3.0	Yes		Anterior and posterior saturation bands, NSA = 2	(19)
Torso	3.0	3D FSE	2830 / 649	125	-	448 x 448	0.9 x 0.9 x 0.8		Respiratory gated		(58)

Peripheral	1.5	T_2/T_1 weighted 3D bSSFP	4 / 1.9	-	-	224 x 192	1.8 x 2.1 x 2.0	Yes	ECG triggered	Partial Fourier	(20)
Peripheral	1.5	3D FSE 3D Dixon	4000 / 884 4233 / 76	90 -	3-5 3:30	512 x 288 320 x 192	0.8 x 1.4 x 0.8-1.4 1.2 x 2.0 x 6.0			Driven equilibrium -	(51)
Peripheral	1.5	3D FSE 3D Dixon	4000 / 884 4233 / 76	90	- -	- -	- -				(84)
Peripheral	1.5	3D TSE	2000 / 694	180	4:04	256 x 256	2.0 x 1.9 x 1.7				(85–88)
Peripheral	1.5	3D TSE (SPACE)	4000 / 221	120	-	-	1.0 x 1.4 x 1.5	Yes		Parallel imaging acceleration factor = 3	(23)
Peripheral	3.0	3D TSE	2820 / 740	-	-	240 x 190	1.5 x 1.5 x 2.0			Partial Fourier	(28, 89–91)
Peripheral	3.0	3D TSE	3600 / 80	90	-	320 x 304	1.15 x 1.05 x 5	Yes			(92)
Peripheral	3.0	3D TSE	3000 / 600	110	10:51	-	1.39 x 1.39 x 3.0	Yes		Anterior and posterior saturation bands, NSA = 2	(19)
Peripheral	3.0	3D TSE	2500 / 650	-	-	-	1.6 x 1.9 x 2.8	Yes		Partial Fourier, parallel imaging acceleration factor = 1.9	(36)
Peripheral	3.0	TSE	3690 / 80	-	-	352 x 256	0.9 x 1.2 x 6.0				(24)
Peripheral	3.0	3D FSE	2830 / 649	125	-	448 x 448	0.9 x 0.9 x 0.8				(58)
Peripheral	3.0	STIR	5940 / 90	120	-	-	1.8 x 1.3 x 3			Parallel imaging acceleration	(25)

										factor = 2, TI = 180	
Peripheral	3.0	3D RARE	5940 / 90	120	-	-	1.8 x 1.3 x 3			Parallel imaging acceleration factor = 2, TI = 180	(30)
Peripheral	3.0	RARE	-	-	-	-	-				(5)
Peripheral	3.0	Flow weighted ASL	- / 4	-	40	-	3 x 3 x 5	Yes		TI = 3500 – 10000, NSA = 8 *, Partial Fourier, parallel imaging acceleration factor = 2	(9)

TOF – time of flight; RARE – Rapid acquisition with relaxation enhancement; STIR – short tau inversion recovery; TSE/FSE – turbo/fast spin echo; bSSFP – balanced steady state free precession; ASL – arterial spin labelling; NSA – number of signal averages

Table 2. Contrast enhanced studies. All studies are T_1-weighted unless otherwise stated. Where field of view and matrix are present, but voxel sizes not stated, calculated voxel sizes are displayed. The Fat Suppressed column indicates if a fat suppression pre-pulse was used; Dixon imaging or water frequency selective excitations is not considered as such.
** - study included a single participant imaged in the torso which is not detailed here.*
† - varies with anatomy; representative value given
‡ - echo time optimised per participant. Note also that for MRL without the addition of an USPIO TR/TE1/TE = 4.4 - 4.5/ 1.2 - 1.5/2.4 - 2.7 ms.
§ - described within the source as T_1 weighted despite the sequence parameters

Anatomical region	**Field strength (T)**	**Sequence variant**	**TR/TE (ms)**	**Flip angle (°)**	**Acquisition time (s)**	**Resolution**		**Additional parameters**			**Source**
						In-Plane Matrix	**Reconstructed Voxel (mm)**	**Fat Suppressed?**	**Motion Reduction**	**Other**	
Head and Neck	1.5	3D SPGR (SMMT)	27.5 / 8.5	50	-	512 x 192	-				(21)
Head and Neck	1.5	-	5.01 / 1.03	30	-	195 x 256	1.5 x 0.9 x 1.3				(42)
Torso	1.5	3D SPGR	4.6 / 1.2	15	32 - 42	256 x 128	1.7 x 3.0 – 3.4 x 2.0	Yes	Breath-hold		(60)
Torso	1.5	3D SPGR (THRIVE)	4.0 / 1.9	10	20 - 30	-	0.65-1 x 0.65-1, 1-1.3	Yes	Breath-hold	Partial Fourier, Parallel imaging acceleration factor = 2 - 4	(40)
Torso	1.5	MRA (TWIST) 3D IR-FLASH	3 / 1 300 / 1.5	25 20	900 -	320 x 240 320 x 240	1.2 x 1.2 x 1.2 1.2 x 1.2 x 1.2		Navigator gated		(41, 59)
Torso	1.5	3D Dixon	'shortest' / 1.8, 4.0	15	10 per stack (3 stacks required to image entire torso)	-	1.0 x 1.0 x 1.0		Breath-hold	Parallel imaging acceleration factor = 1.65	(64)
Peripheral *	1.5	3D GRE	5.1/1.4	30	~ 180 †	256 x 192	~ 0.7 x 0.6 x 1.4 †			NSA = 2	(10)

Peripheral	1.5	3D GRE	4.8/1.4	30	-	- / -					(93)
Peripheral	1.5	3D SPGR (VIBE)	3.4/1.47	25	44	448 x 448	2.2 x 1.1 x 1.5				(85, 88)
Peripheral	1.5	3D SPGR (VIBE)	3.58 / 1.47	35	100	448 x 448	1.2 x 1.1 x 1.2				(86, 87)
Peripheral	1.5	3D SPGR (FLASH)	5.1 / 1.23	25	31	448 x 448	2.0 x 1.0 x 1.0				(37)
Peripheral	1.5	3D SPGR	6.14 / 2.77	12	78		1 x 1 x 1	Yes			(8)
Peripheral	1.5	3D SPGR	5.0 / 2.1	25	250	448 x 320	1.0 x 1.4 x 2.8	Yes			(20)
Peripheral	1.5 and 3.0		5.60 / 1.86	-	-	-	- / - / 0.5				(94)
Peripheral	3.0	3D GRE	5.7 / 2.5	70	120	380 x 70	1.1 x 5.7	Yes			(81)
Peripheral	3.0	3D SPGR (FLASH)	4.13/1.47	25	149	448 x 448	0.8 x 0.8 x 0.8	Yes		Parallel imaging acceleration factor = 3	(25)
Peripheral	3.0	3D SPGR (THRIVE)	3.5 / 1.7	25	40	300 x 256	1.5 x 1.2 x 1.2	Yes		NSA = 2	(28, 90, 92)
Peripheral	3.0	3D SPGR (THRIVE)	3.5 / 1.7	25	180	300 x 256	1.4 x 0.5 x 0.5	Yes			(33)
Peripheral	3.0	3D SPGR (THRIVE)	23 / 2.1	15	180	760 x 720	0.5 x 0.5 x 1.3			Parallel imaging acceleration factor = 2, NSA = 2	(92)
Peripheral	3.0	3D SPGR (THRIVE)	6.4 / 1.7	100	130	300 x 256	1.2 x 1.2	Yes			(24)
Peripheral	3.0	3D SPGR (THRIVE) §	2820 / 740	25	60	240 x 190	1.5 x 1.0 x 1.0	Yes		NSA = 2	(95)
Peripheral	3.0	3D SPGR	3.5 / 1.7	25	180	750 x 640	1.2 x 0.5	Yes			(96)
Peripheral	3.0	3D SPGR (FLASH)	3.5 / 1.3	14.9	70	228 x 202	1.0 x 1.4 x 1.2	Yes		Parallel imaging acceleration factor = 2,	(23)

Peripheral	3.0	3D SPGR (FLASH)	4.13 / 1.47	25	149	448 x 448	0.8 x 0.8 x 0.8	Yes		Parallel imaging acceleration factor = 3	(30)
Peripheral	3.0	3D SPGR	4.13 / 1.47	25	149	448 x 448	0.8 x 0.8 x 0.8	Yes		NSA = 3	(5)
Peripheral	3.0	3D FSE (VISTA) 3D proton density weighted FSE (VISTA)	350 / 17 1400 / 40	- -	227 284		1 x 1 x 1 1 x 1 x 1	Yes Yes		Parallel imaging acceleration factor = 2 - 2.5 Parallel imaging acceleration factor = 2 – 2.5; Driven Equilibrium	(52)
Peripheral	3.0	3D Dixon	- / optimised, optimised ‡	20	60 - 90	~ 220x 220 †	~ 1.4 x 1.4 x 1.8 †			Venous suppression with USPIO	(97)
Peripheral	3.0	3D Dixon	'shortest' / optimised, optimised ‡	20	-	-	-			Venous suppression with USPIO	(36)

SPGR – spoilt gradient echo; GRE – gradient echo; TSE/FSE – turbo/fast spin echo; NSA - number of signal averages; MRA – magnetic resonance angiography; USPIO – ultra-small superparamagnetic iron oxide; SMMT - spectral-spatial excitation magnetization transfer

Table 3. Contrast Injection and massage protocols in contrast enhanced studies. Standard concentrations of each agent, in mol/L, are: Gadopentetate dimeglumine, 0.5; gadoteridol, 0.5; gadobutrol, 1.0; gadoterate meglumine, 0.5; gadodiamide, 0.5; gadobenate dimeglumine, 0.5.
** - Repeated between or during data acquisition.*
† - dilution with saline doubled in 'younger' participants
‡ - per injection site
§ - active ingredient mepivacaine hydrochloride

Anatomical region	**Field strength (T)**	**Contrast agent(s)**	**# of injections**	**Location of injection**	**Injection solution**		**Injection volume (per site)**	**Massage of injection site**	**Source**
					GBCA vol.	**Other added**			
Head and Neck	1.5	Gadoteridol Gadopentetate dimeglumine	variable	variable	variable	variable	≤1 mL	variable	(21)
Head and Neck	1.5	Gadopentetate dimeglumine	5	bilateral submucosa of the pharyngeal recess	4.5 mL	0.5 mL LH (2%)	1 mL	1 min	(42)
Torso	1.5	Gadopentetate dimeglumine	2	peri areolar	1.0 mL	0.25 mL LH (1%)	0.5 mL	-	(60)
Torso	1.5	Gadopentetate dimeglumine	2	inguinal LNs	0.1 mmol/kg	equal volume of saline †	-	-	(40)
Torso	1.5	Gadopentetate dimeglumine	2	inguinal LNs	variable	-	2-8 mL	-	(41, 59)
Torso	1.5	Gadobutrol	4	digital webspaces	6.0 mL	2 mL saline (post 0.2 mL 1% MH)	1 mL	-	(64)
Peripheral	1.5	Gadoterate meglumine	5	webspaces + medial to 1st distal metatarsal	4.5 mL	0.5 mL LH (2%)	1 mL	2 min	(10)
Peripheral	1.5	Gadodiamide	5	digital webspaces + medial to 1st proximal phalanx	4.5 mL	0.5 mL MH (1%)	1 mL	1 min *	(37)
Peripheral	1.5	Gadodiamide	5	digital webspaces + medial to 1st proximal phalanx	18 mL	2 mL MH (1%)	2 mL	1 min *	(88)
Peripheral	1.5	Gadodiamide	5	digital webspaces + medial to 1st proximal phalanx	0.1 mmol/kg	2 mL MH (1%)	≤1.8 mL	1 min *	(85)

Peripheral	1.5	Gadodiamide	5	digital webspaces + medial to 1st proximal phalanx	9.0 mL	1 mL MH (1%)	2 mL	-	(86)
Peripheral	1.5	Gadobutrol	5	digital webspaces + dorsal area of foot	4.5 mL	0.5mL LH (2%)	1 mL	5 min	(93)
Peripheral	1.5	Gadoteridol	5	digital webspaces + medial to 1st proximal phalanx	18 mL	2 mL MH (1%)	2 mL	-	(87)
Peripheral	1.5	Gadoteridol	4	digital webspaces	0.9 mL ‡ 0.02 mL ‡	0.1 mL LH (1%) 0.1 mL LH (1%) + 0.88 mL saline	1 mL	-	(8)
Peripheral	1.5	Gadobenate dimeglumine	4	digital webspaces	0.1 mL/kg	1 mL LH (2%)	≤1 mL	-	(20)
Peripheral	1.5 and 3.0	Gadodiamide	variable	variable	12-20 mL	4 mL LH (2%)	variable	0.5 min	(94)
Peripheral	3.0	Gadobenate dimeglumine	4	digital webspaces	15 mL	1.5 mL LH (1%)	0.7-0.8 mL	-	(28)
Peripheral	3.0	Gadobenate dimeglumine	-	-	-	-	0.7-0.8 mL	-	(89)
Peripheral	3.0	Gadobenate dimeglumine	4	digital webspaces	8.0 mL	1 mL MH (1%)	1.1 mL	-	(91)
Peripheral	3.0	Gadobenate dimeglumine	4	digital webspaces	-	10:1 ratio GBCA:LH (1%)	1 mL	0.5 min	(92)
Peripheral	3.0	Gadobenate dimeglumine	1	base of scrotum	-	10:1 ratio GBCA:LH (10%)	0.5 mL	0.5 min	(96)
Peripheral	3.0	Gadobenate dimeglumine	4	digital webspaces	-	-	0.7-0.8 mL	-	(90)
Peripheral	3.0	Gadobenate dimeglumine	2	2nd and 4th digital webspaces	0.8 mL	0.2 mL scandinibsa §	1 mL	-	(81)
Peripheral	3.0	Gadobenate dimeglumine Ferumoxytol	4 -	digital webspaces intravenous	5.0 mL 5 mg/kg	1 mL LH (1%) Saline dilution to 60 mL total volume	1 mL 60 mL	-	(97)
Peripheral	3.0	Gadobenate dimeglumine Ferumoxytol	4 -	digital webspaces Intravenous	5.0 mL 5 mg/kg	1 mL LH (1%) Saline dilution to 60 mL total volume	1 mL 60 mL		(36)

Peripheral	3.0	Gadopentetate dimeglumine	3	digital webspaces	5.5 mL	0.5 mL MH (1%)	1 mL	0.5 min	(33)
Peripheral	3.0	Gadopentetate dimeglumine	3	1st three digital webspaces	5.4 mL	0.6 mL MH	1 mL	2 min	(25)
Peripheral	3.0	Gadopentetate dimeglumine	3	1st three digital webspaces	5.4 mL	0.6 mL MH	1 mL	2 min	(30)
Peripheral	3.0	Gadopentetate dimeglumine	3	1st three digital webspaces	-	MH	1 mL	2 min	(5)
Peripheral	3.0	Gadopentetate dimeglumine	4	digital webspaces	15 mL	1.5 mL LH (1%)	0.7-0.8 mL	2 min	(24)
Peripheral	3.0	Gadopentetate dimeglumine	3	three finger digital webspaces	5.5 mL	0.5 mL MH (1%)	1 mL	0.5 min	(95)
Peripheral	3.0	Gadobutrol	3	1st three digital webspaces	0.1 mmol/kg	0.5 mL LH (1%)	≤2 mL	1 min	(52)
Peripheral	3.0	Gadobutrol	4	digital webspaces	4.5 mL	0.5 mL LH	1 mL	2 min	(23)

LH - lidocaine hydrochloride; MH - mepivacaine hydrochloride

Table 4. Summary of commonly reported findings presented in each study. The subject column details the affected cohort, except when only healthy volunteers were enrolled. All articles include some reference to the presence or morphology of LVs (e.g. shape, dilation and tortuosity). Note that, despite not being specifically lymphatic, the presence of a honeycomb pattern in the soft tissue is included here given the frequency of reporting.

Anatomical region	**Field strength (T)**	**Subjects**	**Qualitative Measurements**			**Quantitative Measurements**			**Source**
			Dermal Rerouting	**Fluid Accumulation**	**Other**	**Size**	**Signal**	**Other**	
Head and Neck	1.5	Healthy volunteers			LV and blood signal intensity with protocol variations		LN enhancement ratio vs time	LN count	(21)
Head and Neck	1.5	Nasopharyngeal carcinoma							(42)
Head and Neck	3.0	Healthy volunteers			Presence of meningeal LVs				(29)
Torso	1.5	Healthy volunteers				LN diameter: mean = 4.1 ± 2.2 mm (sentinel node), = 4.3 ± 0.8 (distal nodes)	Normalised LV and LN signal vs time	LN count	(60)
Torso	1.5	Liver disease and malignancy				TD diameter: mean = 4.23 ± 1.76 mm in affected participant, 3.74 ± 0.81 mm in healthy volunteers			(56)
Torso	1.5	Functional single-ventricle palliation surgery		Yes	Collateral LVs	TD diameter: range = 1.3-7.2 and 1.7-2.6mm in surgical and non-single-ventricle heart disease participants			(57)
Torso	1.5	Central conducting lymphatic anomalies		Yes	Collateral LVs, retrograde flow, LV occlusion and lymph leakage				(40)
Torso	1.5	Congenital heart disease			Retrograde flow				(59)
Torso	1.5	Plastic Bronchitis			LV occlusion and retrograde flow				(41)

Torso	1.5	Chylous effusions		Yes	Retrograde flow and lymph leakage				(64)
Torso	3.0	Healthy volunteers							(83)
Torso	3.0	BCRL		Yes		Max LV area: 17.2 ± 15.6 mm^2 in the affected side of participants, 8.7 ± 2.1 and 8.7 ± 2.8 mm^2 in the left and right side of healthy volunteers	Lymphatic SNR		(19)
Torso	3.0	Fontan circulation		Yes	Collateral LVs	TD: diameter: mean = 2.7 ± 1.1mm in both affected and unaffected participants TD relative length: mean = 1.12 ± 0.09 mm in affected, 1.05 ± 0.04 mm in unaffected volunteers			(58)
Peripheral	1.5	Lymphoceles		Yes	LV leakage		LV and LN SNR vs time		(10)
Peripheral	1.5	Lower limb lymphoedema	Yes		Collateral LVs	Max LV diameter: 5 mm	Time to maximal LV, LN and venous signal intensity		(85)
Peripheral	1.5	Lower limb lymphoedema	Yes			Max LV diameter: 5 mm	Time to maximal LV, LN and venous signal intensity		(37)
Peripheral	1.5	Lymphoceles	Yes	Yes	LV leakage	Max LV diameter: 5 mm	LV and vein signal vs time		(88)
Peripheral	1.5	Lower limb lymphoedema	Yes	Yes	Collateral LVs	LV diameter: range = 1 – 5 mm	LV, LN and vein SNR vs time		(86)
Peripheral	1.5	Lower limb lymphoedema		Yes	Relative LV count				(93)
Peripheral	1.5	Lower limb lymphoedema		Yes	LV Occlusion, collateral LVs	LV diameter: range = 1 – 5 mm	LN enhancement vs time		(87)

Peripheral	1.5	Lower limb lymphoedema		Yes	Honeycomb pattern			LN count	(51)
Peripheral	1.5	BCRL			Visibility of injection site and blood signal intensity with protocol variations		LV and vein signal vs time	LV speed = 9.7, 2.1 cm/min in a healthy and affected limb	(8)
Peripheral	1.5	Upper or Lower limb lymphoedema and BCRL	Yes	Yes	Honeycomb pattern, collateral LVs	Mean LV diameter: 2.2 ± 0.5 and 1.5 ± 0.2 in in affected and unaffected limbs respectively	LV SNR vs time	LV count	(20)
Peripheral	1.5 and 3.0	Cervical cancer							(94)
Peripheral	3.0	Lymphoedema, lymphoceles or LV transplant	Yes	Yes			LV and venous SNR and CNR		(25)
Peripheral	3.0	Lymphoedema or LV transplant	Yes						(30)
Peripheral	3.0	Lower limb lymphoedema	Yes	Yes		LV diameter: range = 1.2 – 8 mm	LN SNR vs time	LV and LN count: LV range 1 – 'numerous' lymph speed: range = 0.3 – 1.48 cm/min	(28)
Peripheral	3.0	Lower limb lymphoedema	Yes	Yes	Honeycomb pattern, collateral LVs	Max LV diameter: 4.28 ± 1.53 and 3.41 ± 1.05 in T_2-w and CE-T_1 images respectively	LV SNR and CNR	LV count: mean = 6.82 ± 5.10, 4.88 ± 4.18, in T_2-w and CE-T_1 images respectively)	(91)
Peripheral	3.0	Lower limb lymphoedema		Yes		LV diameter: range = 0.5 – 8 mm		LV count: range = 0 to 'numerous'	(89)
Peripheral	3.0	Lower limb lymphoedema	Yes			LV diameter: median = 3.41 ± 1.4, 2.49 ± 0.79 mm and 2.11 ± 1.25, 1.29 ± 0.35 mm in affected and unaffected calf and thigh respectively		LV count: median = 7, 10 and 5, 5 mm in unaffected and affected calf and thigh respectively	(33)
Peripheral	3.0	Lower limb lymphoedema	Yes						(5)

Peripheral	3.0	Lower limb lymphoedema	Yes		Honeycomb pattern	LN diameter	LN enhancement ratio vs time		(24)
Peripheral	3.0	Upper or Lower limb lymphoedema	Yes		More LV observed in T_1 vs PD weighted images				(52)
Peripheral	3.0	Upper or lower limb lymphoedema	Yes		Reduction in venous signal with USPIO injection.		LV signal and LV to muscle contrast ratio as a function of TE (signal reduced by 45% and contrast by 21% in long TE sequence)		(36)
Peripheral	3.0	Upper or lower limb lymphoedema	Yes		LV location				(81)
Peripheral	3.0	Upper limb lymphoedema	Yes			LV diameter: mean = 3.06 ± 0.78 vs 1.98 ± 0.30 mm in affected participant vs healthy controls			(23)
Peripheral	3.0	BCRL						Lymph Speed = 0.48 ± 0.15 and 0.58 ± 0.16 cm/min if affected vs unaffected cases	(9)
Peripheral	3.0	BCRL	Yes	Yes	LV leakage	LV diameter: range = 0.5 – 5 mm		LV count: median = 4	(90)
Peripheral	3.0	BCRL		Yes					(84)
Peripheral	3.0	BCRL			Collateral LVs	Max LV area: 12.9 ± 6.3 mm^2 in the affected side of participants, 8.8 ± 4.2 and 8.4 ± 1.6 mm^2 in the left and right side of healthy volunteers	Lymphatic SNR		(19)
Peripheral	3.0	BCRL	Yes	Yes	Honeycomb pattern, LV leakage	LV diameter: mean = 1.73 ± 0.24, 0.65 ± 0.36 mm in			(95)

						affected participant vs healthy controls			
Peripheral	3.0	Inguinal lymphatic vessel leakage		Yes	Honeycomb pattern, LV leakage		SNR in LV leakage site and LNs	Leaking LV count: range = 1 – 5 (median = 2)	(92)
Peripheral	3.0	Genital lymphoedema	Yes	Yes			LN signal vs time	LV count	(96)
Peripheral	3.0	Fontan circulation	Yes						(58)
Peripheral	3.0				LV and blood signal intensity with protocol variations				(97)

LV – lymphatic vessel; LN – lymph node; SNR – signal-to-noise ratio; CNR – contrast-to-noise ratio; BCRL – breast cancer related lymphoedema; USPIO – Ultrasmall superparamagnetic Iron Oxide

References

1. Lymphedema [https://www.ncbi.nlm.nih.gov/books/NBK537239/]

2. Földi M, Földi E: *Földi's Textbook of Lymphology for Physicians and Lymphoedmema Therapists*. 3rd ed. München: Urban & Fischer; 2012.

3. Schulze H, Nacke M, Gutenbrunner C, Hadamitzky C: Worldwide assessment of healthcare personnel dealing with lymphoedema. *Health Econ Rev* 2018; 8.

4. The International Society of Lymphology (ISL): THE DIAGNOSIS AND TREATMENT OF PERIPHERAL LYMPHEDEMA: 2020 CONSENS US DOCUMENT OF THE INTERNATIONAL SOCIETY OF LYMPHOLOGY. *Lymphology* 2020; 53:3–19.

5. Weiss M, Burgard C, Baumeister R, et al.: Magnetic resonance imaging versus lymphoscintigraphy for the assessment of focal lymphatic transport disorders of the lower limb. *Nuklearmedizin* 2014; 53:190–196.

6. Liu NF, Lu Q, Liu PA, Wu XF, Wang BS: Comparison of radionuclide lymphoscintigraphy and dynamic magnetic resonance lymphangiography for investigating extremity lymphoedema. *Br J Surg* 2010; 97:359–365.

7. Mihara M, Hara H, Araki J, et al.: Indocyanine Green (ICG) lymphography is superior to lymphoscintigraphy for diagnostic imaging of early lymphedema of the upper limbs. *PLoS One* 2012; 7:1–9.

8. Borri M, Schmidt MA, Gordon KD, et al.: Quantitative Contrast-Enhanced Magnetic Resonance Lymphangiography of the Upper Limbs in Breast Cancer Related Lymphedema: An Exploratory Study. *Lymphat Res Biol* 2015; 13:100–106.

9. Rane S, Donahue PMC, Towse T, et al.: Clinical feasibility of noninvasive visualization of lymphatic flow with principles of spin labeling MR imaging: implications for lymphedema assessment. *Radiology* 2013; 269:893–902.

10. Ruehm SG, Schroeder T, Debatin JF: Interstitial MR lymphography with gadoterate meglumine: Initial experience in humans. *Radiology* 2001; 220:816–821.

11. Liu NF, Yu Z, Luo Y, Sun D, Yan Z: A novel FLT4 gene mutation and MR lymphangiography in a Chinese family with Milroy disease. *Lymphology* 2015; 48:93–96.

12. Liu NF, Yu ZY, Sun D, Lou Y: Rare variants in LAMA5 gene associated with FLT4 and FOXC2 mutations in primary lymphedema may contribute to severity. *Lymphology* 2016; 49:192–204.

13. White RD, Weir-Mccall JR, Budak MJ, Waugh SA, Munnoch DA, Sudarshan TAP: Contrast-enhanced magnetic resonance lymphography in the assessment of lower limb lymphoedema. *Clin Radiol* 2014; 69:e435–e444.

14. Lohrmann C, Bartholomä JP, Foeldi E, Speck O, Langer M: Magnetic resonance lymphangiography in Klippel-Trénaunay syndrome. *Br J Radiol*

2007; 80:188–192.

15. Kim EY, Hwang HS, Lee HY, et al.: Anatomic and functional evaluation of central lymphatics with noninvasive magnetic resonance lymphangiography. *Med (United States)* 2016; 95:1–8.

16. Moher D, Liberati A, Tetzlaff J, Altman DG: Academia and Clinic Annals of Internal Medicine Preferred Reporting Items for Systematic Reviews and Meta-Analyses : *Ann Intern Med* 2009; 151:264–269.

17. Downs SH, Black N: The feasibility of creating a checklist for the assessment of the methodological quality both of randomised and non-randomised studies of health care interventions. *J Epidemiol Community Health* 1998; 52:377–384.

18. Quality Assessment Tool for Case Series Studies [https://www.nhlbi.nih.gov/health-topics/study-quality-assessment-tools]

19. Crescenzi R, Donahue PMC, Hartley KG, et al.: Lymphedema evaluation using noninvasive 3T MR lymphangiography. *J Magn Reson Imaging* 2017; 46:1349–1360.

20. Mazzei MA, Gentili F, Mazzei FG, et al.: High-resolution MR lymphangiography for planning lymphaticovenous anastomosis treatment: a single-centre experience. *Radiol Medica* 2017; 122:918–927.

21. Loo BW, Draney MT, Sivanandan R, et al.: Indirect MR lymphangiography of the head and neck using conventional gadolinium contrast: A pilot study in humans. *Int J Radiat Oncol Biol Phys* 2006;

66:462–468.

22. Ruehm SG, Corot C, Debatin JF: Interstitial MR lymphography with a conventional extracellular gadolinium-based agent: Assessment in rabbits. *Radiology* 2001; 218:664–669.

23. Bae JS, Yoo RE, Choi SH, et al.: Evaluation of lymphedema in upper extremities by MR lymphangiography: Comparison with lymphoscintigraphy. *Magn Reson Imaging* 2018; 49(December 2017):63–70.

24. Zhou GX, Chen X, Zhang JH, Zhu JQ, Wang Y Bin, Wang ZQ: MR lymphangiography at 3.0 Tesla to assess the function of inguinal lymph node in low extremity lymphedema. *J Magn Reson Imaging* 2014; 40:1430–1436.

25. Notohamiprodjo M, Baumeister RGH, Jakobs TF, et al.: MR-lymphangiography at 3.0T - A feasibility study. *Eur Radiol* 2009; 19:2771–2778.

26. Hadjis NS, Carr DH, Banks L, Pflug JJ: The role of CT in the diagnosis of primary lymphedema of the lower limb. *Am J Roentgenol* 1985; 144:361–364.

27. Crescenzi R, Donahue PM, Braxton VG, et al.: 3.0 T relaxation time measurements of human lymph nodes in adults with and without lymphatic insufficiency: Implications for magnetic resonance lymphatic imaging. *NMR Biomed* 2018; 31:1–11.

28. Liu N-FF, Lu Q, Jiang Z-HH, Wang C-GG, Zhou J-GG: Anatomic and

functional evaluation of the lymphatics and lymph nodes in diagnosis of lymphatic circulation disorders with contrast magnetic resonance lymphangiography. *J Vasc Surg* 2009; 49:980–987.

29. Kuo PH, Stuehm C, Squire S, Johnson K: Meningeal Lymphatic Vessel Flow Runs Countercurrent to Venous Flow in the Superior Sagittal Sinus of the Human Brain. *Tomography* 2018; 4:99–104.

30. Notohamiprodjo M, Weiss M, Baumeister RG, et al.: MR Lymphangiography at 3.0 T: Correlation with Lymphoscintigraphy. *Radiology* 2012; 264:78–87.

31. Mitsumori LM, McDonald ES, Neligan PC, Maki JH: Peripheral Magnetic Resonance Lymphangiography: Techniques and Applications. *Tech Vasc Interv Radiol* 2016; 19:262–272.

32. Olszewski WL, Liu NF: Magnetic Resonance Lymphography (MRL): Point and counter-point. *Lymphology* 2013; 46:202–207.

33. Lu Q, Delproposto Z, Hu A, et al.: MR Lymphography of Lymphatic Vessels in Lower Extremity with Gynecologic Oncology-Related Lymphedema. *PLoS One* 2012; 7:3–8.

34. Mitsumori LM, McDonald ES, Wilson GJ, Neligan PC, Minoshima S, Maki JH: Mr lymphangiography: How i do it. *J Magn Reson Imaging* 2015; 42:1465–1477.

35. Maki JH, Neligan PC, Briller N, Mitsumori LM, Wilson GJ: Dark Blood Magnetic Resonance Lymphangiography Using Dual-Agent Relaxivity

Contrast (DARC-MRL): A Novel Method Combining Gadolinium and Iron Contrast Agents. *Curr Probl Diagn Radiol* 2016; 45:174–179.

36. Ripley B, Wilson GJ, Lalwani N, Briller N, Neligan PC, Maki JH: Initial clinical experience with dual-agent relaxation contrast for isolated lymphatic channel mapping. *Radiology* 2018; 286:705–714.

37. Lohrmann C, Foeldi E, Langer M: Indirect magnetic resonance lymphangiography in patients with lymphedema preliminary results in humans. *Eur J Radiol* 2006; 59:401–6.

38. Case TC, Witte CL, Witte MH, Unger EC, Williams WH: Magnetic resonance imaging in human lymphedema: Comparison with lymphangioscintigraphy. *Magn Reson Imaging* 1992; 10:549–558.

39. Hayashi S, Miyazaki M: Thoracic duct: visualization at nonenhanced MR lymphography--initial experience. *Radiology* 1999; 212:598–600.

40. Krishnamurthy R, Hernandez A, Kavuk S, Annam A, Pimpalwar S: Imaging the central conducting lymphatics: Initial experience with dynamic MR lymphangiography. *Radiology* 2015; 274:871–878.

41. Itkin MG, McCormack FX, Dori Y: Diagnosis and treatment of lymphatic plastic bronchitis in adults using advanced lymphatic imaging and percutaneous embolization. *Ann Am Thorac Soc* 2016; 13:1689–1696.

42. Qiuhang Z, Zhenlin W, Yan Q, Jun H, Yongfeng S, Bo H: Lymphatic drainage of the skull base: comparative anatomic and advanced imaging studies in the rabbit and human with implications for spread of

nasopharyngeal carcinoma. *Lymphology* 2010; 43:98–109.

43. Taoka T, Naganawa S: Glymphatic imaging using MRI. *J Magn Reson Imaging* 2020; 51:11–24.

44. Jiang Q: MRI and glymphatic system. *Stroke Vasc Neurol* 2019; 4:75–77.

45. Nedergaard M, Goldman SA: Brain drain. *Sci Am* 2016; 314:45–49.

46. Aspelund A, Antila S, Proulx ST, et al.: A dural lymphatic vascular system that drains brain interstitial fluid and macromolecules. *J Exp Med* 2015; 212:991–999.

47. Hershenhouse KS, Shauly O, Gould DJ, Patel KM: Meningeal Lymphatics: A Review and Future Directions From a Clinical Perspective. *Neurosci Insights* 2019; 14:117906951988902.

48. Margaris KN, Black RA: Modelling the lymphatic system: Challenges and opportunities. *J R Soc Interface* 2012; 9:601–612.

49. BERNSTEIN MA, KING KF, Zhou XJ: *Handbook of MRI Pulse Sequences*. 1st edition. London: Elsevier; 2004.

50. Hargreaves BA, Gold GE, Lang PK, et al.: MR imaging of articular cartilage using driven equilibrium. *Magn Reson Med* 1999; 42:695–703.

51. Arrivé L, Derhy S, Dahan B, et al.: Primary lower limb lymphoedema: classification with non-contrast MR lymphography. *Eur Radiol* 2018; 28:291–300.

52. Jeon JY, Lee SH, Shin MJ, Chung HW, Lee MH: Three-dimensional

isotropic fast spin-echo MR lymphangiography of T1-weighted and intermediate-weighted pulse sequences in patients with lymphoedema. *Clin Radiol* 2016; 71:e56–e63.

53. Telinius N, Drewsen N, Pilegaard H, et al.: Human thoracic duct in vitro: Diameter-tension properties, spontaneous and evoked contractile activity. *Am J Physiol - Hear Circ Physiol* 2010; 299:811–818.

54. Olszewski WL, Engeset A: Intrinsic contractility of prenodal lymph vessels and lymph flow in human leg. *Am J Physiol - Hear Circ Physiol* 1980; 8:775–783.

55. Lustig M, Donoho D, Pauly JM: Sparse MRI: The application of compressed sensing for rapid MR imaging. *Magn Reson Med* 2007; 58:1182–1195.

56. Takahashi H, Kuboyama S, Abe H, Aoki T, Miyazaki M, Nakata H: Clinical Feasibility of Noncontrast- Enhanced Magnetic Resonance Lymphography of the Thoracic Duct. *Chest* 2003; 124:2136–2142.

57. Dori Y, Keller MS, Fogel MA, et al.: MRI of lymphatic abnormalities after functional single-ventricle palliation surgery. *Am J Roentgenol* 2014; 203:426–431.

58. Mohanakumar S, Telinius N, Kelly B, et al.: Morphology and Function of the Lymphatic Vasculature in Patients With a Fontan Circulation. *Circ Cardiovasc Imaging* 2019; 12:e008074.

59. Dori Y, Keller MS, Rome JJ, et al.: Percutaneous lymphatic embolization

of abnormal pulmonary lymphatic flow as treatment of plastic bronchitis in patients with congenital heart disease. *Circulation* 2016; 133:1160–1170.

60. Suga K, Yuan Y, Ogasawara N, Okada M, Matsunaga N: Localization of breast sentinel lymph nodes by MR lymphography with a conventional gadolinium contrast agent: Preliminary observations in dogs and humans. *Acta radiol* 2003; 44:35–42.

61. Korteweg MA, Zwanenburg JJM, Van Diest PJ, et al.: Characterization of ex vivo healthy human axillary lymph nodes with high resolution 7 Tesla MRI. *Eur Radiol* 2011; 21:310–317.

62. Ledger AEW, Borri M, Pope RJE, et al.: Investigating the influence of flip angle and k-space sampling on dynamic contrast-enhanced MRI breast examinations. *Acad Radiol* 2014; 21:1394–1401.

63. Eggers H, Brendel B, Duijndam A, Herigault G: Dual-echo Dixon imaging with flexible choice of echo times. *Magn Reson Med* 2011; 65:96–107.

64. Pieper CC, Schild HH: Interstitial Transpedal MR-Lymphangiography of Central Lymphatics Using a Standard MR Contrast Agent: Feasibility and Initial Results in Patients with Chylous Effusions. *RoFo Fortschritte auf dem Gebiet der Rontgenstrahlen und der Bildgeb Verfahren* 2018; 190:938–945.

65. Fortuin AS, Philips BWJ, van der Leest MMG, et al.: Magnetic resonance imaging at ultra-high magnetic field strength: An in vivo assessment of number, size and distribution of pelvic lymph nodes. *PLoS One* 2020; 15(7

July):1–10.

66. Philips BWJ, Stijns RCH, Rietsch SHG, et al.: USPIO-enhanced MRI of pelvic lymph nodes at 7-T: preliminary experience. *Eur Radiol* 2019; 29:6529–6538.

67. Freitag MT, Breithaupt M, Berger M, et al.: In vivo visualization of mesoscopic anatomy of healthy and pathological lymph nodes using 7T MRI: A feasibility study. *J Magn Reson Imaging* 2015; 41:1405–1412.

68. Gennaro P, Chisci G, Mazzei F, Gabriele G: Magnetic resonance lymphangiography: How to prove it? *J Magn Reson Imaging* 2016:509–510.

69. Bieri O, Scheffler K: Fundamentals of balanced steady state free precession MRI. *J Magn Reson Imaging* 2013; 38:2–11.

70. Pharmacovigilance Risk Assessment Committee European Medicines Agency: Assessment report. Gadolinium containing contrast agents. 2017; 44(July).

71. Misselwitz B: MR contrast agents in lymph node imaging. *Eur J Radiol* 2006; 58:375–382.

72. Moore JE, Bertram CD: Lymphatic System Flows. *Annu Rev Fluid Mech* 2018; 50:459–482.

73. Swartz MA: The physiology of the lymphatic system. *Adv Drug Deliv Rev* 2001; 50:3–20.

74. Nganga EC, Gitau S, Makhdomi K: Lower limb lymphoscintigraphy

patterns among patients with lower limb lymphedema: a pictorial essay. *Clin Transl Imaging* 2018; 6:135–143.

75. Pappalardo M, Cheng MH: Lymphoscintigraphy for the diagnosis of extremity lymphedema: Current controversies regarding protocol, interpretation, and clinical application. *J Surg Oncol* 2020; 121:37–47.

76. Gray RJ, Worsley PR, Voegeli D, Bader DL: Monitoring contractile dermal lymphatic activity following uniaxial mechanical loading. *Med Eng Phys* 2016; 38:895–903.

77. Franconeri A, Ballati F, Panzuto F, et al.: A proposal for a semiquantitative scoring system for lymphedema using Non-contrast Magnetic Resonance Lymphography (NMRL): Reproducibility among readers and correlation with clinical grading. *Magn Reson Imaging* 2020; 68(February):158–166.

78. Partsch H: Assessment of abnormal lymph drainage for the diagnosis of lymphedema by isotopic lymphangiography and by indirect lymphography. *Clin Dermatol* 1995; 13:445–450.

79. Li W, Liu P, Lu H, Strouse JJ, van Zijl PCM, Qin Q: Fast measurement of blood T1 in the human carotid artery at 3T: Accuracy, precision, and reproducibility. *Magn Reson Med* 2017; 77:2296–2302.

80. Kousi E, Smith J, Ledger AE, et al.: Quantitative evaluation of contrast agent uptake in standard fat-suppressed dynamic contrast-enhanced MRI examinations of the breast. *Med Phys* 2018; 45:287–296.

81. Pons G, Clavero JA, Alomar X, Rodríguez-Bauza E, Tom LK, Masia J: Preoperative planning of lymphaticovenous anastomosis: The use of magnetic resonance lymphangiography as a complement to indocyanine green lymphography. *J Plast Reconstr Aesthetic Surg* 2019; 72:884–891.

82. Cellina M, Martinenghi C, Panzeri M, et al.: Noncontrast MR Lymphography in Secondary Lower Limb Lymphedema: *J Magn Reson Imaging* 2020:1–9.

83. Chen S, Tan X, Wu R, et al.: Non-enhanced MR lymphography of the thoracic duct: improved visualization following ingestion of a high fat meal–initial experience. *Clin Physiol Funct Imaging* 2017; 37:730–733.

84. Arrivé L, Derhy S, Dlimi C, El Mouhadi S, Monnier-Cholley L, Becker C: Noncontrast Magnetic Resonance Lymphography for Evaluation of Lymph Node Transfer for Secondary Upper Limb Lymphedema. *Plast Reconstr Surg* 2017; 140:806e-811e.

85. Lohrmann C, Foeldi E, Speck O, Langer M: High-resolution MR lymphangiography in patients with primary and secondary lymphedema. *Am J Roentgenol* 2006; 187:556–561.

86. Lohrmann C, Foeldi E, Bartholomä J-P, Langer M: Magnetic Resonance Imaging of Lymphatic Vessels Without Image Subtraction. *J Comput Assist Tomogr* 2007; 31:303–308.

87. Lohrmann C, Pache G, Felmerer G, Foeldi E, Schaefer O, Langer M: Posttraumatic edema of the lower extremities: Evaluation of the lymphatic

vessels with magnetic resonance lymphangiography. *J Vasc Surg* 2009; 49:417–423.

88. Lohrmann C, Felmerer G, Speck O, Keck T, Foeldi E, Langer M: Postoperative lymphoceles: Detection with high-resolution MR lymphangiography. *J Vasc Interv Radiol* 2006; 17:1057–1062.

89. Liu NF, Yan ZX, Wu XF: Classification of lymphatic-system malformations in primary lymphoedema based on MR lymphangiography. *Eur J Vasc Endovasc Surg* 2012; 44:345–349.

90. Liu NF, Wang BS: Functional lymphatic collectors in breast cancer-related lymphedema arm. *Lymphat Res Biol* 2014; 12:232–237.

91. Lu Q, Xu J, Liu N: Chronic lower extremity lymphedema: A comparative study of high-resolution interstitial MR lymphangiography and heavily T2-weighted MRI. *Eur J Radiol* 2010; 73:365–373.

92. Lu Q, Bui D, Liu NF, Xu JR, Zhao XH, Zhang XF: Magnetic resonance lymphography at 3T: A promising noninvasive approach to characterise inguinal lymphatic vessel leakage. *Eur J Vasc Endovasc Surg* 2012; 43:106–111.

93. Dimakakos EP, Koureas A, Koutoulidis V, et al.: Interstitial magnetic resonance lymphography: The clinical effectiveness of a new method. *Lymphology* 2008; 41:116–125.

94. Hong Y, Xiang L, Hu Y, Zhou Z, Yu H, Zhu B: Interstitial magnetic resonance lymphography is an effective diagnostic tool for the detection of

lymph node metastases in patients with cervical cancer. *BMC Cancer* 2012; 12.

95. Sheng L, Zhang G, Li S, Jiang Z, Cao W: Magnetic Resonance Lymphography of Lymphatic Vessels in Upper Extremity with Breast Cancer-Related Lymphedema. *Ann Plast Surg* 2020; 84:100–105.

96. Lu Q, Jiang Z, Zhao Z, et al.: Assessment of the lymphatic system of the genitalia using magnetic resonance lymphography before and after treatment of male genital lymphedema. *Med (United States)* 2016; 95:1–8.

97. Maki JH, Neligan PC, Briller N, Mitsumori LM, Wilson GJ: Dark Blood Magnetic Resonance Lymphangiography Using Dual-Agent Relaxivity Contrast (DARC-MRL): A Novel Method Combining Gadolinium and Iron Contrast Agents. *Curr Probl Diagn Radiol* 2016; 45:174–179.